SECURITY CLASSIFICATION OF THIS PAGE

(2)

REPORT DOCUMENTATION PAGE

1a. REPORT SECURITY CLASSIFICATION
Unclassified

2a. SECURITY CLASSIFICATION AUTHORITY

AD-A229 918

2b. DECLASSIFICATION / DOWNGRADING SCHEDULE

4. PERFORMING ORGANIZATION REPORT NUMBER(S)
ONR Technical Report #13

5. MONITORING ORGANIZATION REPORT NUMBER(S)

6a. NAME OF PERFORMING ORGANIZATION
Dept of Chemical Engineering and Materials Science

6b. OFFICE SYMBOL (If applicable)
Code 1113

7a. NAME OF MONITORING ORGANIZATION
Office of Naval Research

6c. ADDRESS (City, State, and ZIP Code)
University of Minnesota
Minneapolis, MN 55455

7b. ADDRESS (City, State, and ZIP Code)
800 North Quincy Street
Arlington, VA 22217

DTIC ELECTE DEC14 1990 S E D

8a. NAME OF FUNDING / SPONSORING ORGANIZATION
Office of Naval Research

8b. OFFICE SYMBOL (If applicable)

9. PROCUREMENT INSTRUMENT IDENTIFICATION NUMBER
Contract No. N00014-87-K-0494

8c. ADDRESS (City, State, and ZIP Code)
800 North Quincy Street
Arlington, VA 22217-5000

10 SOURCE OF FUNDING NUMBERS

PROGRAM ELEMENT NO.	PROJECT NO.	TASK NO.	WORK UNIT ACCESSION NO

11. TITLE (Include Security Classification)
Voltammetric Measurement of Bimolecular Electron-Transfer Rates in Low Ionic Strength Solutions

12. PERSONAL AUTHOR(S)
John D. Norton, Wendy E. Benson, Henry S. White, Bradford D. Pendley and Hector D. Abruna

13a. TYPE OF REPORT	13b. TIME COVERED	14. DATE OF REPORT (Year, Month, Day)	15. PAGE COUNT
Technical	FROM 1/1/90 TO 10/31/90	11/16/90	

16. SUPPLEMENTARY NOTATION
submitted to **Analytical Chemistry**, November 1990

17 COSATI CODES		
FIELD	GROUP	SUB-GROUP

18. SUBJECT TERMS (Continue on reverse if necessary and identify by block number)

19. ABSTRACT (Continue on reverse if necessary and identify by block number)

Numerical analysis of the sequential electron-transfer mechanism, $A \rightarrow A^+ + e^-$, $A^+ \rightarrow A^{2+} + e^-$ demonstrates that the rate at which A can be directly oxidized to A^{2+} is inhibited in low ionic strength solutions by the coupled diffusion-migration of chemically-generated A^+. The latter species, A^+, is produced within the depletion layer by the homogeneous reaction, $A + A^{2+} \overset{k_b}{\rightleftharpoons} 2A^+$, and is electrostatically repelled from electrode surface, thereby reducing the flux of A at the electrode surface. Steady-state voltammetric currents corresponding to two examples of this reaction mechanism, the oxidation of tetrathiafulvalene (TTF) and the reduction of tetracyanoquinodimethane (TCNQ), have been measured at platinum microdisk electrodes over a wide range of electrolyte concentrations (0 - 0.1 M). Analyses of the mass-transfer limited currents provide a lower limit of 10^6 $M^{-1}s^{-1}$ for the bimolecular reaction rate constants, k_b, for $TTF + TTF^{+2} \overset{k_b}{\rightarrow} 2TTF^+$ and $TCNQ + TCNQ^{2-} \overset{k_b}{\rightarrow} 2TCNQ^-$.

20. DISTRIBUTION / AVAILABILITY OF ABSTRACT
☒ UNCLASSIFIED/UNLIMITED ☐ SAME AS RPT ☐ DTIC USERS

21. ABSTRACT SECURITY CLASSIFICATION
Unclassified

22a. NAME OF RESPONSIBLE INDIVIDUAL
Henry S. White

22b. TELEPHONE (Include Area Code)
(612) 625-6995

22c. OFFICE SYMBOL

DD FORM 1473, 84 MAR 83 APR edition may be used until exhausted. All other editions are obsolete

SECURITY CLASSIFICATION OF THIS PAGE

VOLTAMMETRIC MEASUREMENT OF BIMOLECULAR ELECTRON-TRANSFER RATES IN LOW IONIC STRENGTH SOLUTIONS

John D. Norton, Wendy E. Benson, and Henry S. White*
Department of Chemical Engineering and Materials Science
University of Minnesota
Minneapolis, MN 55455

Bradford D. Pendley and Héctor D. Abruña*
Department of Chemistry
Baker Laboratory
Cornell University
Ithaca, NY 14853

ABSTRACT. Numerical analysis of the sequential electron-transfer mechanism,

$$A \rightarrow A^+ + e^-$$

$$A^+ \rightarrow A^{2+} + e^-$$

demonstrates that the rate at which A can be directly oxidized to A^{2+} is inhibited in low ionic strength solutions by the coupled diffusion of A and diffusion-migration of chemically-generated A^+. The latter species, A^+, is produced within the depletion layer by the homogeneous reaction, $A + A^{2+} \xrightarrow{k_b} 2A^+$, and is electrostatically repelled from the electrode surface, thereby reducing the flux of A at the electrode surface. Steady-state voltammetric currents corresponding to two examples of this reaction mechanism, the oxidation of tetrathiafulvalene (TTF) and the reduction of tetracyanoquinodimethane (TCNQ), have been measured at platinum microdisk electrodes over a wide range of electrolyte concentrations (0 - 0.1 M). Analyses of the mass-transfer limited currents provide a lower limit of 10^6 $M^{-1}s^{-1}$ for the bimolecular reaction rate constants, k_b, for $TTF + TTF^{+2} \xrightarrow{k_b} 2TTF^+$ and $TCNQ + TCNQ^{2-} \xrightarrow{k_b} 2TCNQ^-$.

Submitted to *Analytical Chemistry*, November, 1990.

BRIEF. Steady-state voltammetry at platinum microdisk electrodes is used to estimate rate constants of bimolecular electron-transfer reactions.

INTRODUCTION.

Electrochemical investigations of homogeneous chemical reactions that are coupled to an initial electron-transfer step are frequently based on methods in which the mass-transfer coefficient of a reactant or intermediate is experimentally varied relative to the inherent rate of the chemical reaction. Common methods employed in studying coupled chemical reactions include the rotating disk electrode (RDE)[1], rotating ring-disk electrode (RRDE)[2], and cyclic voltammetry[3]. In the RDE and RRDE experiments, the rate of mass-transfer is proportional to the square-root of the electrode rotation rate, $\omega^{1/2}$, so that the mass-transfer rate may be adjusted to a value comparable to the rate of the chemical reaction. The dependence of the limiting current on $\omega^{1/2}$ in this experimental regime may be analyzed, using appropriate kinetic equations[4], to determine the rate constant of a chemical reaction. In cyclic voltammetry at a stationary electrode, the rate at which the electrode potential is scanned, ν, between two potential limits controls the instantaneous mass-transfer rate. The scan rate can be varied in a fashion completely analogous to the rotation rate in the RDE experiment, providing an analytical method to observe short-lived intermediates and to quantitatively measure the rates of chemical reactions.

Fleischmann[5,6,7], Murray,[8] Rusling[9], and coworkers have applied similar reasoning in developing steady-state voltammetric methods using microdisk electrodes for measuring the rate constants of coupled homogenous reactions. In analogy to varying the rotation rate of a RDE or the scan rate in a cyclic voltammetric experiment, these workers based their analysis on the dependence of the mass-transfer rate on the electrode size. Because of the near-convergent flux of species to a microdisk, the rate of mass-transfer to or away from a microdisk is inversely proportional to the electrode radius. For example, in a report by Fleischmann and coworkers[6], an analysis of the limiting current of voltammetric waves, using platinum microdisk electrodes of radii between 0.3 and 25 μm, yielded first order and psuedo-first order rate constants as large as ~10^3 s^{-1}, although these authors estimated that values as large as 10^5 s^{-1} could be obtained from steady-state voltammetry. Both

values compare favorably with the magnitude of first order rate constants evaluated by ultra-fast microelectrode voltammetry[10]. In addition, the measurement of steady-state transport-limited currents requires much simpler instrumentation and completely avoids the difficulties in correcting for the large capacitive currents observed at high scan rates.

In this report, the influence of electric fields on the mass-transfer rate of charged chemical intermediates is examined. We demonstrate that migration of chemical intermediates can have a pronounced effect on steady-state limiting currents observed at microdisk electrodes in solutions in which the bulk concentration of supporting electrolyte, C_{elec}, is comparable to or smaller than the concentration of redox species, C_{redox}. Although migrational fluxes have been considered for over half a century in the analysis of electrode reactions[11], we are not aware of any previous reports in which this effect has been exploited in kinetic studies of coupled chemical reactions. The kinetic studies described here are concerned with bimolecular electron-transfer reactions coupled to an initial electron-transfer reaction. The key experimental parameter in the analysis, which is analogous to ω in the RDE experiment or v in cyclic voltammetry, is the ratio C_{elec}/C_{redox}. Using 10-20 μm radius microdisk electrodes, we show that bimolecular reaction rates of 10^6 $M^{-1}s^{-1}$ can be readily determined by steady-state measurement of limiting currents. Generalization of this method to other electrode reaction mechanisms is considered.

EXPERIMENTAL.

Tetrathiafulvalene (TTF, Sigma) and tetracyanoquinodimethane (TCNQ, Aldrich) were used as received. Acetonitrile (Burdick and Jackson, distilled in glass) was dried over activated 4 Å molecular sieves. Tetra-n-butylammonium perchlorate (TBAP, GF Smith) was recrystallized 3 times from ethyl acetate and dried under vacuum.

Pt microdisk electrodes were prepared by two methods detailed in earlier reports. In the first method[12], a 2 cm length of a nominally 12.5 μm radius Pt wire (Goodfellow, 99.9%) was attached to the end of a copper wire with Ag paint (Acme) and subsequently

encased in the tip of a glass pipet with epoxy ("white epoxi-patch", Dexter Corp., Olean, NY). The tip of the electrode was ground flat with 600 grit emery paper to expose the cross-section of the Pt wire. The second method consisted of sealing a previously constructed microelectrode[13] in a 3mm od glass tube and successively polishing with 400 and 600 grit sandpaper. Prior to each experiment, the electrode was polished with 1μm diamond paste (Buehler). Similar results were obtained using both methods of electrode preparation. Precise values of the electrode radii were calculated from values of the limiting voltammetric currents for 1-5 mM ferrocene oxidation in CH_3CN containing 0.1 M TBAP using the reported value for the diffusivity of ferrocene in CH_3CN (2.4×10^{-5} cm^2/s)[14]

Electrochemical measurements were made using a conventional three-electrode cell. A sodium saturated calomel electrode (SSCE) or a Ag-wire quasi-reference electrode[12] (0.2 $\pm$ 0.1 V vs. SSCE) was used as the reference electrode. All potentials are reported vs SSCE. A Pt wire was used as the counterelectrode. Voltammetric curves were obtained using either a Princeton Applied Research Corp. Model 173 potentiostat and Model 175 Universal Programmer or an IBM EC/225 Voltammetric Analyzer and were made inside a Faraday cage.

Digital Simulations. The computer simulations utilize a finite-difference method with an exponentially expanding space grid[15,16] to simulate the time dependent flux and spatial distribution of ions at a hemi-spherical electrode of radius, r_o. A large, concentric, hemi-spherical counter electrode is assumed, which maintains a radial flux to the microelectrode at all times.

Initially, the neutral reactant and the supporting electrolyte (if present) are assumed to exist at their respective uniform bulk concentrations. At time, t=0, the surface concentrations of the reactant (A) and monovalent species (A^+ or A^-) are set equal to zero, corresponding to an overpotential sufficient to cause the mass-transfer limited two-electron oxidation (or reduction) of A. The homogeneous bimolecular reaction between A and A^{2+}

(or A^{2-}) is incorporated in the simulation following prescribed methods[4]. The simulation is allowed to run until steady-state concentration profiles and fluxes are obtained, generally requiring a dimensionless time, $Dt/r_o^2 = 10$. Simulations were performed using an IBM XT microcomputer.

RESULTS and DISCUSSION.

Figure 1 shows representative cyclic voltammograms obtained at a nominally 12.5 μm radius Pt disk electrode in CH_3CN containing 5 mM TTF and varying amounts of supporting electrolyte (TBAP). The two sigmoidally-shaped waves with $E_{1/2}$ values at 0.20 and 0.56V vs SSCE in CH_3CN/0.1 M TBAP correspond to the one and two-electron oxidations of TTF respectively:

$$TTF \rightarrow TTF^{+} + e^{-} \quad (1)$$

$$TTF \rightarrow TTF^{2+} + 2e^{-} \quad (2)$$

The magnitude of the current for the first wave, (eq. (1)) varies slightly (< 10%) with TBAP concentration but is in good agreement with the theoretical value expected for a diffusion controlled reaction at an inlaid disk. The flux under this condition is given by

$$i = 4nFDC_{redox}r_o \quad (3)$$

where C_{redox} is the bulk concentration of TTF, r_o is the electrode radius, F is Faraday's constant, n is the number of electrons transferred per molecule, and D is the diffusion constant for TTF. From eq. (3), and measurements of the limiting current for the first wave, we estimate $D = (2.2 \pm 0.3) \times 10^{-5}$ cm^2/s.

The second oxidation of TTF, (eq. (2)), is much more sensitive to the electrolyte concentration. The height of the second wave, measured relative to the plateau of the first

wave, is expected to be exactly equal to that for the first wave if the reaction is limited by diffusion of TTF to the electrode surface. However, we observe that the limiting current is only 42 % of the first wave in solutions containing no intentionally added electrolyte (Fig. 1C). The magnitude of this second oxidation wave increases as the electrolyte concentration increases, and becomes essentially equal (within 3 %) to that of the first wave when excess supporting electrolyte (0.1 M TBAP) is present in solution (Fig. 1A).

The reduction of TCNQ

$$TCNQ + e^- \rightarrow TCNQ^- \quad (4)$$

$$TCNQ + e^- \rightarrow TCNQ^{2-} \quad (5)$$

at a 16.7 μm radius Pt disk electrode, Fig. 2, parallels the behavior observed for TTF oxidation. The magnitude of the second reduction wave is ~40 % of the first wave in the absence of electrolyte, and the limiting currents are essentially equal when the solution contains excess supporting electrolyte. The first reduction wave yields a diffusivity for TCNQ of $(2.4 \pm 0.2) \times 10^{-5}$ cm^2/s.

The half-wave potentials, $E_{1/2}$, for the oxidation of TTF and reduction of TCNQ are also strongly dependent on the concentration of supporting electrolyte. For example, the first and second reduction waves for TCNQ reduction shift toward negative potentials by 0.26 and 0.59 V, respectively, as the concentration of TBAP is decreased from 0.1 to 0 M (Fig. 2). A similar, but positive, shift in $E_{1/2}$ values for the TTF oxidations is observed. This dependence is attributed primarily to an increase in the solution ohmic resistance as the electrolyte concentration is decreased. A detailed analysis of the dependence of $E_{1/2}$ on electrolyte concentration is described in the preceding article[17]. Variations in the heterogeneous rate constant, the formal redox potential, $E^{o'}$, and liquid junction potentials may also occur as the electrolyte concentration is decreased, thus contributing to the observed dependence of $E_{1/2}$ values on electrolyte concentration.

However, the magnitude of the transport-limited current plateau, which is the focus of the following analysis, is independent of all of these factors.

To explain the unusual dependence of the magnitude of two-electron waves on electrolyte concentration, we propose a mechanism that involves migration of the singly charged ion (TTF^+ or $TCNQ^-$) generated by the homogeneous bimolecular reactions

$$TTF + TTF^{2+} \xrightarrow{k_b} 2TTF^+ \quad (6)$$

$$TCNQ + TCNQ^{2-} \xrightarrow{k_b} 2TCNQ^- \quad (7)$$

that follow the initial two-electron oxidation or reduction of the parent compound (eq. (2) and (5)). The equilibrium constants for these reactions may be calculated using the relationship $K_{eq} = \exp\{(F/RT)(\Delta E^{o'})\}$[4], where $\Delta E^{o'}$ is the difference between the formal potentials of the first and second electron-transfer reactions. Approximating E^o values by voltammetric $E_{1/2}$ values measured in CH_3CN solutions containing 0.1 M TBAP, K_{eq} is calculated to be $10^{6.1}$ for eq. (6) and $10^{9.6}$ for eq. (7). Thus, both reactions are essentially irreversible. To our knowledge, the rate constants of equations (6) and (7) have not been previously measured, but are expected to be essentially diffusion controlled since neither reaction involves bond cleavage nor large solvent or structural reorganization[18]. The rate constants of both reactions are also expected to be independent of ionic concentration since one reactant in each reaction is a neutral species, so that there are no electrostatic work terms to be considered in the expression for the activation energy.

Homogeneous oxidation of the parent compound (TTF) by the product (TTF^{2+}) will produce a thin zone within the depletion layer that contains singly-charged TTF^+ (vide infra). We propose that the diffusional/migrational flux of TTF^+ generated by this reaction governs the magnitude of the second wave.

In solutions in which the concentration of the redox species, C_{redox}, is much less than that of the supporting electrolyte, C_{elec}, TTF^+ generated within the depletion layer (eq.

(6)) diffuses to the electrode surface where it is oxidized back to TTF^{2+}. Addition of the initial heterogeneous step (eq. (2)) and following homogeneous step (eq. (6)) yields eq. (1), with TTF^{+} produced as the final solution product, in accordance with the large equilibrium constant of eq. (6). If the rate constant, k_b, of eq. (6) is sufficiently large, this process will consume essentially all of the TTF before it reaches the electrode surface. The overall reaction, however, yields a two-electron wave regardless of the magnitude of k_b, as expected for a diffusion-controlled process.

In solutions in which the concentration of redox species is comparable to or larger than the electrolyte concentration, i.e., $C_{elec}/C_{redox} \leq 1$, the faradaic generation of charged species (TTF^{+} or TTF^{2+}) produces an electric field within the depletion layer that enhances the flux of TTF^{+} and TTF^{2+} away from the electrode surface[11,19]. This electric field is sufficiently small that it does not effect the equilibrium constants of eqs. (6) and (7). However, TTF^{+} generated in solution (eq. (6)) following the two-electron oxidation of TTF will be electrostatically repelled from the electrode surface instead of diffusing back toward the electrode as occurs in the presence of excess supporting electrolyte. The net effect is a decrease in the current corresponding to the two-electron oxidation of TTF. Note that although this argument leads to the expectation of a decrease in the magnitude of the limiting current for the two-electron process when $C_{redox} > C_{elec}$, the overall coulombic efficiency (electrons transferred per mole of TTF^{+} generated) is independent of the ionic concentration. Completely analogous arguments can be made to account for the decrease in the limiting current for the two-electron reduction of TCNQ in solutions of low ionic strength, Fig. 2.

Finite-difference calculations of the steady-state flux and concentration profiles were performed to test the proposed explanation of the dependence of the limiting currents on electrolyte concentration. A hemi-spherical electrode geometry was assumed in the simulation to avoid the complexity of calculating quasi-radial fluxes to an inlaid disk[20,21,22]. This latter approximation has been shown to be useful for analyses of electron-transfer

reactions that are coupled to complex homogeneous chemical reactions[5-9,23]. The radial fluxes, J_i, of each redox species (TTF, TTF^+, TTF^{2+}) and the electrolyte ions (TBA^+, ClO_4^-) are assumed to be governed by the Nernst-Planck equation, eq. (8),

$$J_i = -D_i \frac{\partial C_i}{\partial r} - \frac{z_i F}{RT} C_i D \frac{\partial \phi}{\partial r} \qquad (8)$$

where $-\left(\frac{\partial \phi}{\partial r}\right)$ is the electric field. Equal diffusivities of all species is assumed.

Numerical values of the ratio of the limiting currents of the second and first oxidation for TTF (or TCNQ reduction), $i_{lim}(2)/i_{lim}(1)$ are shown in Fig. 3 as a function of the ratio of the bulk solution concentration of electrolyte and redox species, C_{elec}/C_{redox}, and as a function of the dimensionless variable $k_b r_o^2 C_{redox}/D$. Using the notation described in Delahay[24], the latter parameter is proportional to $(\delta/\mu)^2$, where δ is the depletion layer thickness and μ is the thickness of the solution reaction zone in which TTF^+ is generated (eq. (6)). The term $k_b r_o^2 C_{redox}/D$ can also be interpreted as the rate of the chemical reaction *within* the depletion layer ($k_b r_o C_{redox}$) relative to the rate of mass-transport (D/r_o).

The sigmoidally-shaped plot of $i_{lim}(2)/i_{lim}(1)$ vs. C_{elec}/C_{redox} at a specified value of $k_b r_o^2 C_{redox}/D$ is anticipated, based on our proposed mechanism, since migration effects are minimized when $C_{elec}/C_{redox} > 1$ and enhanced to a limiting value when $C_{elec}/C_{redox} < 1$. The simulated flux for $k_b r_o^2 C_{redox}/D \geq 10^3$ approaches asymptotic values of $i_{lim}(2)/i_{lim}(1) = 0.43$ as $C_{elec}/C_{redox} \rightarrow 0$ and $i_{lim}(2)/i_{lim}(1) = 1$ as $C_{elec}/C_{redox} \rightarrow \infty$. At values of $k_b r_o^2 C_{redox}/D \leq 0.1$, the homogeneous electron-transfer reaction is too slow to significantly perturb the concentration of redox species within the depletion layer and no diminution of the limiting current for the two-electron reduction is expected (Fig. 3).

Experimental values of $i_{lim}(2)/i_{lim}(1)$ from voltammetric limiting currents for TTF oxidation and TCNQ reduction are plotted in Fig. 3 for comparison to the simulated values. Although the experimental values are systematically lower (~2-4%) than the simulated

curve, the experimental values are in good agreement with the simulation for $k_b r_o^2 C_{redox}/D \geq 10^3$. The data correspond to voltammetric currents measured over a 1000-fold change in C_{elec}/C_{redox}, not including the values of $i_{lim}(2)/i_{lim}(1)$ obtained in the absence of intentionally added supporting electrolyte. Using numerical values of the experimental parameters presented above (r_o, C_{redox}, and D), we estimate from Fig. 3 that $k_b \geq 10^6$ $M^{-1}s^{-1}$ for both eq. (6) and eq. (7).

The small discrepancies between simulated and experimental values of $i_{lim}(2)/i_{lim}(1)$ are wholly due to the assumption employed in the simulations that all solution species have equal diffusivities. Better agreement is obtained by allowing the values of D_{TTF^+} and $D_{TTF^{2+}}$ to be equal to one-half that of D_{TTF} in the simulations. However, as experimental values of D_{TTF^+} and $D_{TTF^{2+}}$ have not been independently verified, we have not incorporated this into our analyses. Variations in the diffusivity of the supporting electrolyte ions have an insignificant effect on $i_{lim}(2)/i_{lim}(1)$.

Simulated steady-state concentration profiles of TTF, TTF^+, and TTF^{2+} for $k_b r_o^2 C_{redox}/D = 10^3$ are shown in Fig. 4 for $C_{elec}/C_{redox} = 20$ (relative excess of electrolyte) and $C_{elec}/C_{redox} = 0$ (no added electrolyte). The curves show that the chemical generation of TTF^+ occurs in a thin reaction zone centered at a distance from the surface of ~0.5 - 1 electrode radii. Conversely, the concentration of the neutral reactant, TTF, is depleted to near-zero values at a similar distance. Comparison of the profiles for $C_{elec}/C_{redox} = 0$ and 20 demonstrates that the concentrations of TTF^+ and TTF^{2+} within this region are markedly smaller in the absence of added electrolyte, consistent with the above mentioned arguments that TTF^+ and TTF^{2+} are electrostatically repelled from the electrode in solutions of low ionic strength.

The concentration profiles shown in Fig. 4 are essentially independent of the bimolecular rate constant used in the simulations when $k_b r_o^2 C_{redox}/D \geq 10^3$. This is a result of the bimolecular reaction going to completion on time scales that are significantly shorter than the time required for either reactant in the homogeneous reaction (TTF or

TTF^{2+}) to diffuse or migrate a distance comparable to the depletion layer thickness. The use of smaller electrodes would shorten the depletion layer thickness, allowing mass-transfer through the depletion layer to occur on a timescale comparable to the chemical reaction. It is obvious that the appropriate choice of electrode radius and redox concentration would allow the bimolecular reaction rates to be measured more precisely than our present measurements allow. Voltammetry at microdisk[13] and microband[25,26] electrodes with dimensions (radius and width, respectively) on the order of a few nanometers have been reported. These electrodes should, in principle, allow measurements of diffusion controlled bimolecular rate constants in CH_3CN ($k_b \sim 2 \times 10^{10}\ M^{-1}s^{-1}$)[27] using the methods described above.

Finally, we note that Kamau and Rusling[28] recently reported a similar study for the reduction of TCNQ as a function of supporting electrolyte concentration. They similarly observed that the limiting current for the second reduction of TCNQ decreased relative to the limiting current for the first reduction as the concentration of supporting electrolyte was decreased. The authors suggested that this dependence could be attributed to the slow rate of $TCNQ^-$ reduction (to $TCNQ^{2-}$) in the absence of an electrolyte. They further postulated that the reduction of $TCNQ^-$ was accelerated by the formation of the ion pair, ($TCNQ^-$ / TBA^+), although no direct evidence of the latter species was presented. As we have demonstrated above, the observed decrease in the second wave can be accounted for without any additional assumptions. Further, the quantitative similarity of the dependencies of $i_{lim}(2)/i_{lim}(1)$ on C_{elec}/C_{redox} (Fig. 3) for TTF oxidation and TCNQ reduction strongly suggests a common mechanism controlling the observed behavior of these systems. Since it is highly unlikely that TTF^+ and $TCNQ^-$ are ion paired to the same extent by the supporting electrolyte anion (ClO_4^-) and cation (TBA^+) and that their further oxidation and reduction, respectively, are activated to the same degree by ion pairing, it is unlikely that the mechanism of Kamau and Rusling can account for the electrochemical behavior of these systems. We also note that the numerical simulations employed here are

based on classical diffusion-migration flux equations. The good agreement between simulation and experiment is the best indicator that the dependence of the two-electron oxidation or reduction wave arises solely from the enhance migration of charged species, and not from any chemical effect(s).

CONCLUSION. A simple voltammetric method has been developed for measuring the rate constants of bimolecular electron-transfer reactions between a neutral redox species and its corresponding divalent cation or anion. The key feature of this method is that the magnitude of the limiting current is strongly dependent on the ratio, C_{elec}/C_{redox}, which can be readily varied over several orders of magnitude for many redox systems. This dependence allows quantitative kinetic information to be extracted from voltammetric curves without varying the scan rate or the electrode size.

Although the numerical results presented here are for a highly specific reaction mechanism, it is clear that limiting voltammetric currents measured for several other electrode reactions that are coupled to homogeneous chemical reactions will depend on the electrolyte concentration. For example, consider the following ECE mechanism

$$A^+ + e^- \rightarrow A \qquad (E)$$

$$A \xrightarrow{k_c} B \qquad (C)$$

$$B + e^- \rightarrow B^- \qquad (E)$$

in which the product of the first electron-transfer, A, undergoes reaction to yield the electroactive species B. In solutions in which $C_{elec}/C_{redox} \leq 1$, the reduction of B to B^- creates a negative charge within the depletion layer, thereby *increasing* the migrational flux

of reactant A^+ to the electrode. Numerical simulations confirm that the above ECE reaction may be enhanced by more than an order of magnitude in the absence of supporting electrolyte[29], the exact enhancement factor depending on the chemical rate constant, k_c, the concentration of B, and C_{elec}/C_{redox}. Thus, it should be possible to quantitatively measure the rate constant of the above ECE mechanism and other reactions by determining the dependence of the limiting current on C_{elec}/C_{redox}. However, because the migrational flux of a specific redox species is dependent on its charge, the dependence of limiting currents on C_{elec}/C_{redox} will generally be more specific to the details of the reaction than what is normally encountered using RDE techniques or cyclic voltammetry in solutions containing excess supporting electrolyte. For instance, numerical simulations show that the steady-state limiting current corresponding to the following ECE reaction

$$A \rightarrow A^+ + e^- \qquad (E)$$

$$A^+ \xrightarrow{k_c} B^+ \qquad (C)$$

$$B^+ \rightarrow B^{2+} + e^- \qquad (E)$$

decreases as the ratio C_{elec}/C_{redox} is decreased, a result of the migration of A^+ and B^+ away from the electrode. This mechanism differs from the above mentioned ECE reaction only in the charges of various chemical species. This highly specific dependence of voltammetric currents on ion charge may prove to be a powerful means for unraveling complex homogeneous chemical reactions that are coupled to electron-transfer events.

CREDITS.

The authors are grateful to Stephen Feldberg for helpful discussions regarding numerical simulations. This work was supported by the Office of Naval Research and the National Science Foundation. H.D.A acknowledges support as an A.P. Sloan Foundation Fellow (1987-1991). B.D.P acknowledges support by an ACS, Division of Analytical Chemistry Fellowship sponsored by the E.I. DuPont Company. W.E.B. acknowledges support through a Summer Undergraduate Research Grant from the Twin Cities Section of the Electrochemical Society.

REFERENCES.

1. Koutecky, J.; Levich, V.G. *Zh. Fiz. Khim.* **1958**, *32*, 1565.
2. Bruckenstein, S.; Miller, B. *Accts. Chem. Res.* **1977**, *10*, 54.
3. Nicholson, R.S.; Shain, I. *Anal. Chem.* **1964**, *36*, 706.
4. Bard, A.J.; Faulkner, L.R. *Electrochemical Methods*; Wiley: New York, 1980 and references within.
5. Fleischmann, M.; Lasserre, F.; Robinson, J.; Swan, D. *J. Electroanal. Chem.* **1984**, *177*, 97.
6. Fleischmann, M.; Lasserre, F.; Robinson, D. *J. Electroanal. Chem.* **1984**, *177*, 115.
7. Denault, G.; Fleischmann, M; Pletcher, D.; Tutty, O.R. *J. Electroanal. Chem.* **1990**, *280*, 243.
8. L. Geng; Murray, R. W. *Inorg. Chem.* **1986**, *25*, 3115.
9. Miaw, C. L.; Rusling, J. F.; Owlia, A. *Anal. Chem.* **1990**, *62*, 268.
10. Howell, J.O.; Wightman, R.M. *J. Phys. Chem.* **1984**, *88*, 3915.
11. Kolthoff, I. M.; Ligane, J. J. *Chem. Rev.* **1939**, *24*, No. 1.
12. Malmsten, R.A.; Smith, C.P. White, H.S. *J. Electroanal. Chem.* **1986**, *215*, 223.
13. Pendley, B.D.; Abruña, H.D. *Anal. Chem.* **1990**, *62*, 782.
14. Kuwana,T.; Bublitz, D.E.; Hoh, G. *J. Am. Chem. Soc.* **1960**, *82*, 5811.
15. Feldberg, S.W. *J. Electroanal. Chem.* **1981**, *127*, 1.
16. Joslin, T.; Pletcher, D. *J. Electroanal. Chem.* **1974**, *49*, 171.
17. Pendley, B.D.; Abruña, H.D.; Norton, J.D.; Benson, W.E. White, H.S. *Anal. Chem.* **1991**, *63*, XXXX.
18. Kowert, B.A.; Marcoux, L.; Bard, A.J. *J. Am. Chem. Soc.* **1972**, *94*, 5538.
19. Norton, J. D.; White, H. S.; Feldberg, S. W., *J. Phys. Chem.*, in press.
20. Hepel, T.; Plot, W.; Osteryoung, J. *J. Phys. Chem.* **1983**, *87*, 1278.
21. Oldham, K.B. *J. Electroanal. Chem.* **1981**, *122*, 1.

22. Heinze, J. *J. Electroanal. Chem.* **1981**, *124*, 73.

23. Dayton, M.A.; Ewing, A.G.; Wightman, R.M. *Anal. Chem.* **1980**, *52*, 2392.

24. Delahay, P. *New Instrumental Methods in Electrochemistry*; Interscience: New York, 1954.

25. Morris, R.B.; Franta, D.J.; White, H.S. *J. Phys. Chem.* **1987**, *91*, 3559.

26. Seibold, J.D.; Scott, E.R.; White, H.S. *J. Electroanal. Chem.* **1989**, *264*, 281.

27. Rehm, D.; Weller, A. *Isr. J. Chem.* **1970**, *8*, 259.

28. Kamau, G.N.; Rusling, J.F. *J. Electroanal. Chem.* **1990**, *292*, 187.

29. Norton, J. D.; and White, H. S. U. Minnesota, unpublished results, 1990.

FIGURES.

1. Cyclic voltammograms for the oxidation of 5 mM TTF in acetonitrile at a 12.5 μm radius Pt disk electrode. Concentration of supporting electrolyte (TBAP): (A) 100 mM; (B) 1 mM; (C) 0 mM.

2. Cyclic voltammograms for the reduction of 5 mM TCNQ in acetonitrile at a 16.7 μm radius Pt disk electrode. Concentration of supporting electrolyte (TBAP): (A) 100 mM; (B) 1 mM; (C) 0 mM. The solutions were purged with N_2.

3. Ratio of the limiting currents for the first and second electron-transfer waves, $(i_{lim}(2)/i_{lim}(1))$, as a function of C_{elec}/C_{redox} and $k_b r_o^2 C_{redox}/D$. The solid line corresponds to computer simulated values. The circles and triangles correspond to experimental values obtained from the oxidation of TTF and reduction of TCNQ. Each data point represents the average value from 2-4 trials.

4. Simulated concentration profiles of TTF, TTF^+, and TTF^{2+} as a function of $C_{elec.}/C_{redox}$. Top: $C_{elec.}/C_{redox} = 20$; bottom: $C_{elec.}/C_{redox} = 0$. A value of $k_b r_o^2 C_{redox}/D = 10^3$ was used in both simulations. Profiles correspond to an electrode potential sufficiently positive to cause the two-electron oxidation of TTF at mass-transfer controlled rates. Concentrations of each species are normalized to the bulk solution concentration of TTF, C_{redox}. The distance from the electrode surface is normalized to the electrode radius, r_o. Analogous concentration profiles are obtained for the $TCNQ/TCNQ^-/TCNQ^{2-}$ redox system.

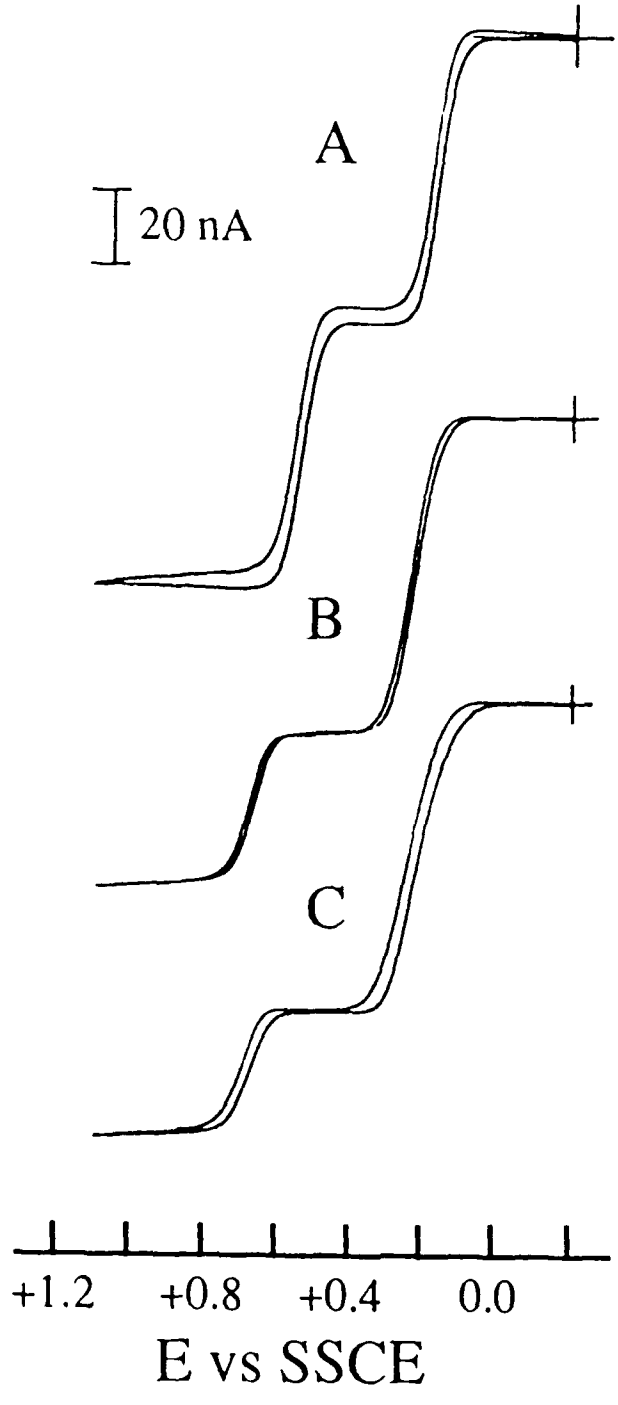

Fig. 1

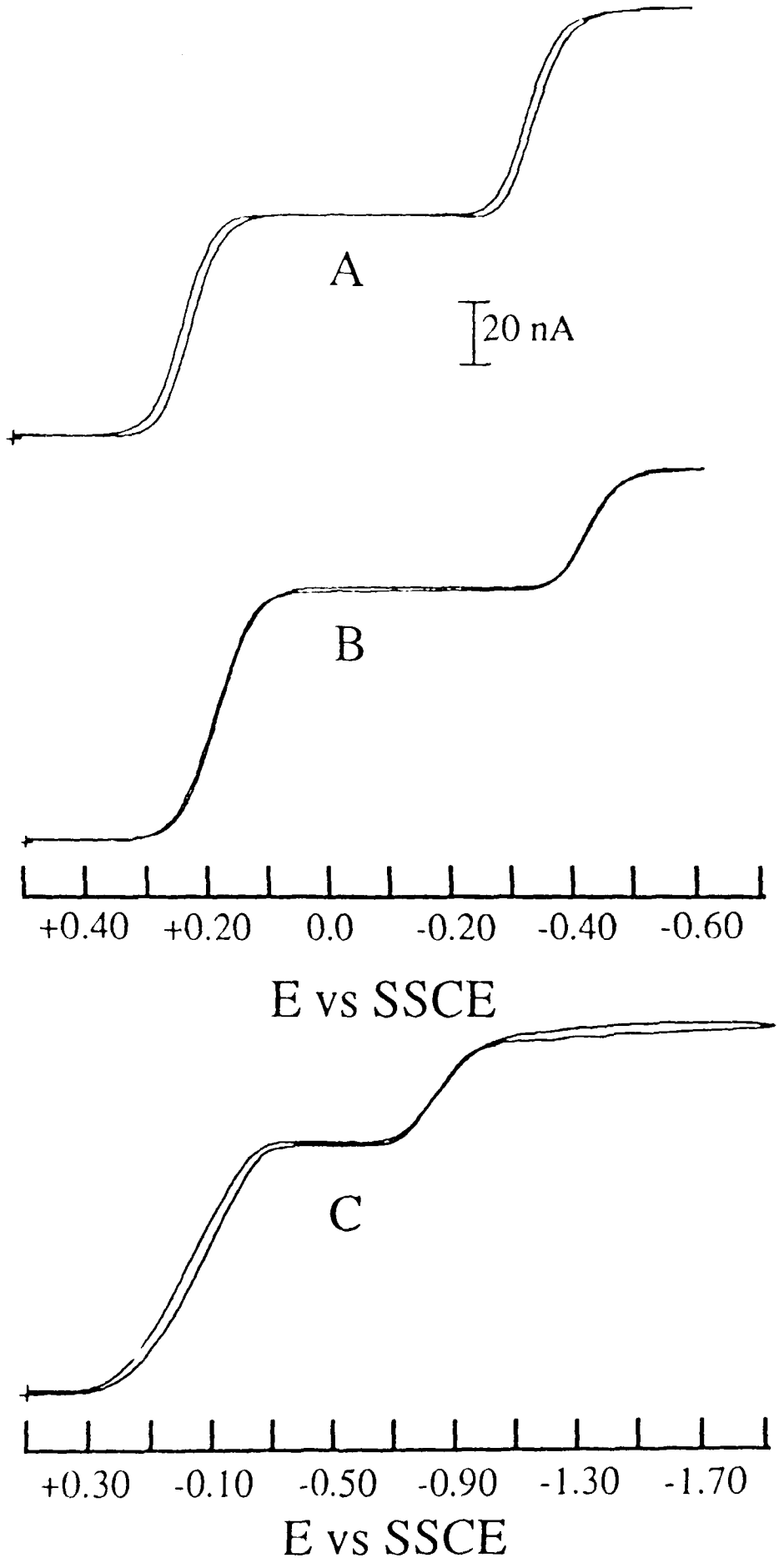
A
20 nA
B
+0.40
+0.20
0.0
-0.20
-0.40
-0.60
E vs SSCE
C
+0.30
-0.10
-0.50
-0.90
-1.30
-1.70
E vs SSCE

Fig.2

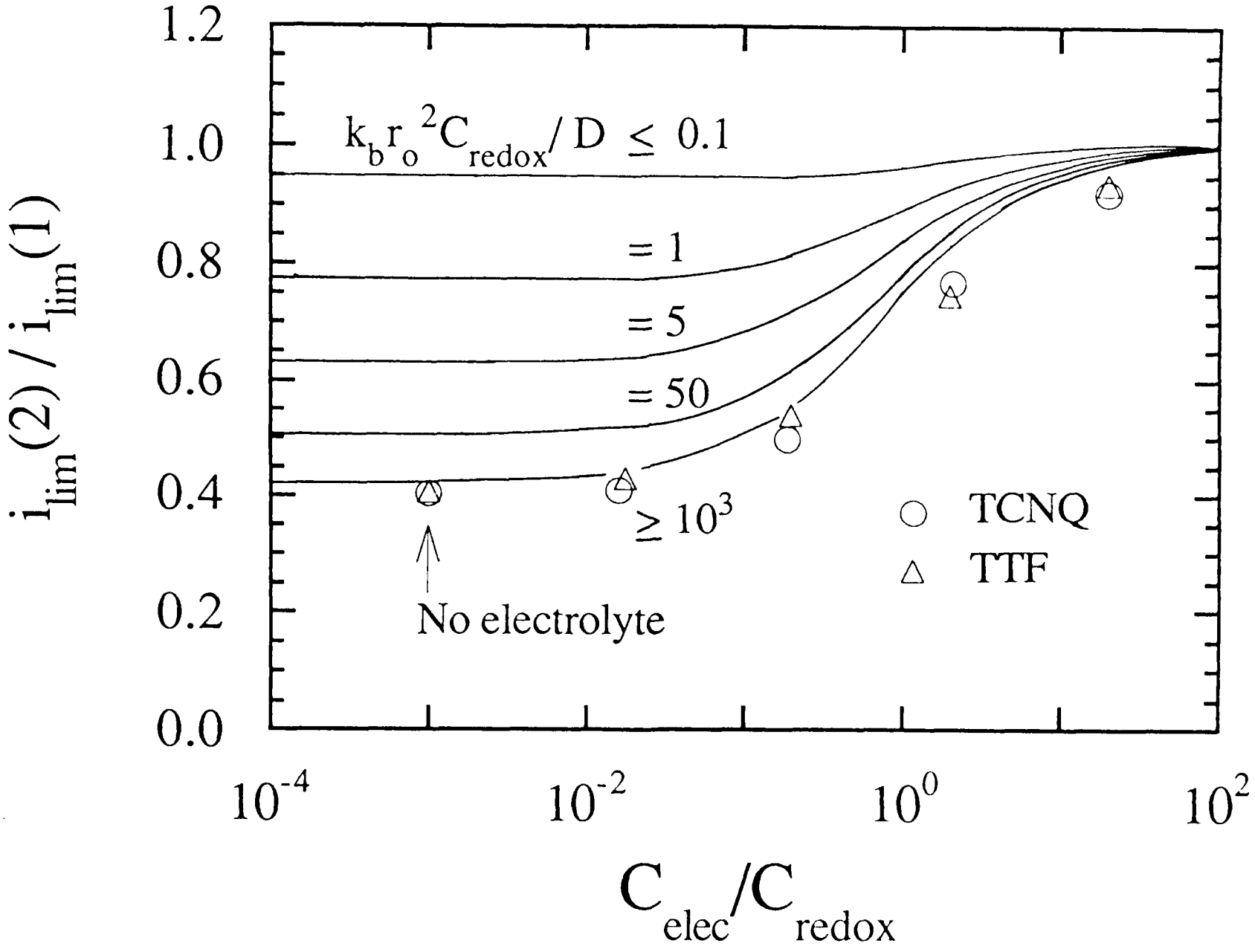
1.2
1.0
0.8
0.6
0.4
0.2
0.0
$i_{lim}(2) / i_{lim}(1)$
$k_b r_o^2 C_{redox} / D \leq 0.1$
= 1
= 5
= 50
$\geq 10^3$
No electrolyte
TCNQ
TTF
10^{-4}
10^{-2}
10^{0}
10^{2}
C_{elec}/C_{redox}

Fig. 3

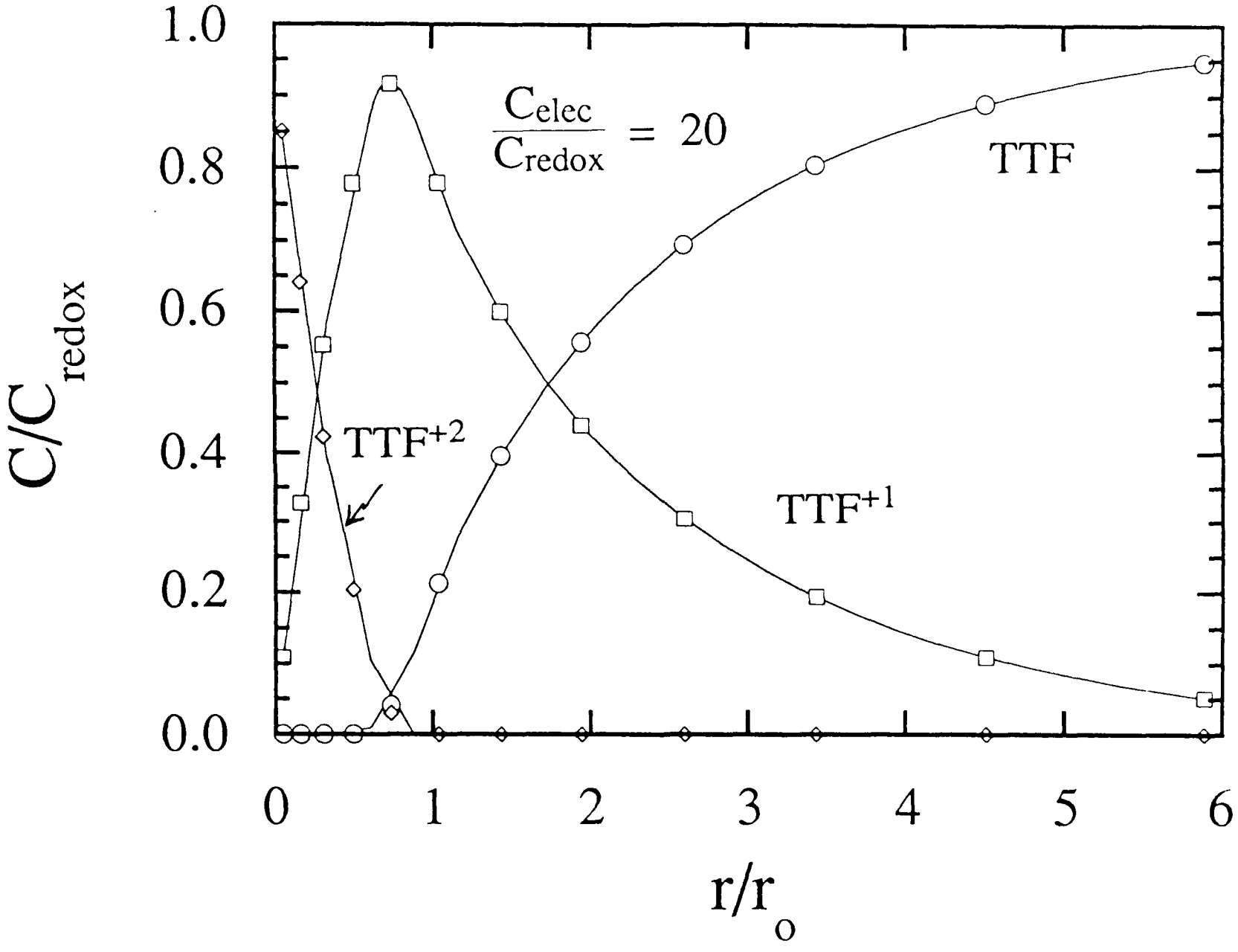
1.0
0.8
0.6
0.4
0.2
0.0
C/C redox
Celec / Credox = 20
TTF
TTF+2
TTF+1
0
1
2
3
4
5
6
r/r o

Fig 4 (top)

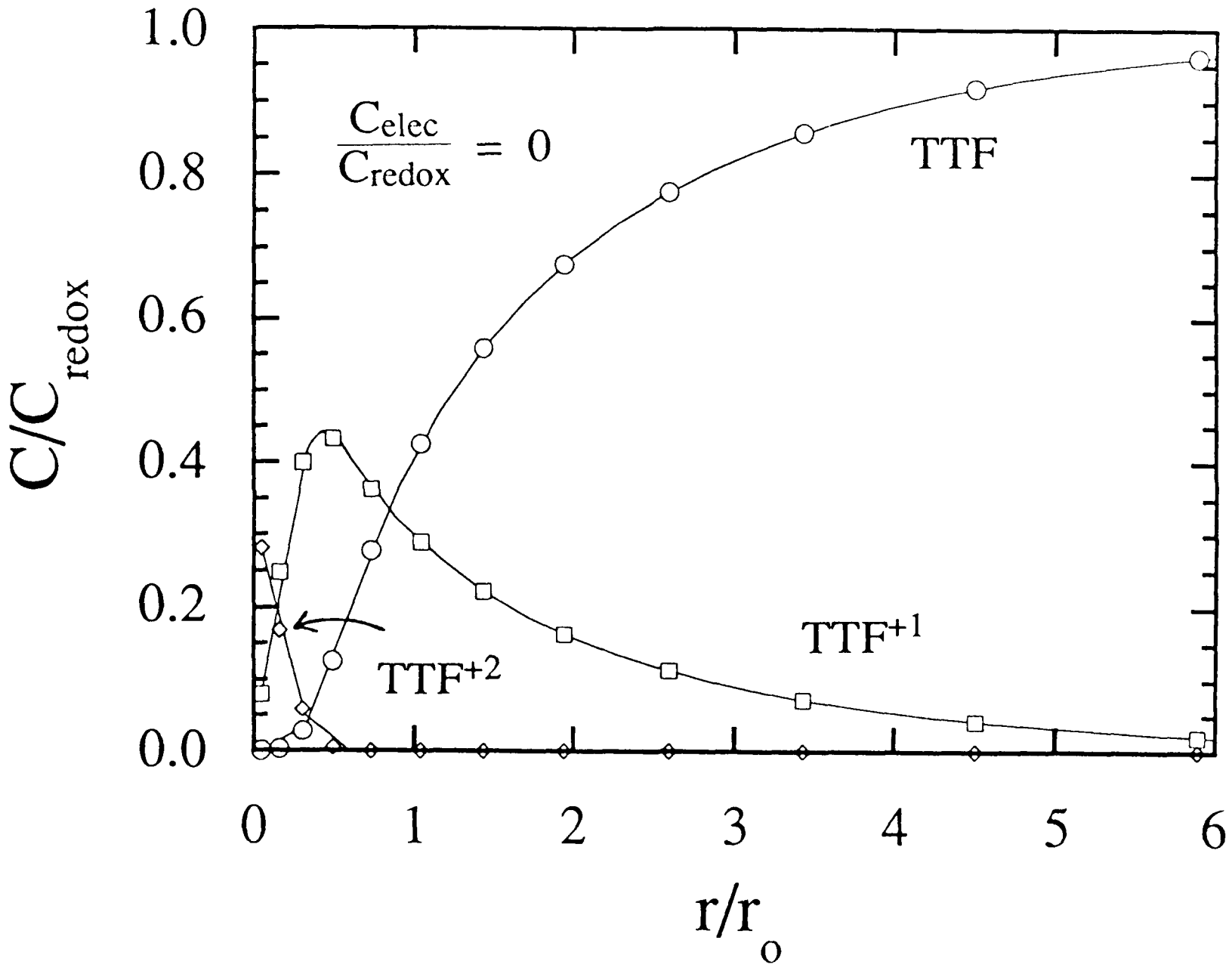
1.0
0.8
0.6
0.4
0.2
0.0
C/C redox
Celec / Credox = 0
TTF
TTF+1
TTF+2
0
1
2
3
4
5
6
r/r o

Fig. 4 (Bottom)